
Nanosized Aluminum as Metal Fuel

The replacement of micrometer-size metal fuel such as aluminum (Al) or boron (B) powders in solid propellants, explosives and pyrotechnics with their nanometer-size counterpart (Nanosized Al) has become a common trend in the design of new types of propellants and solid fuel in recent decades. The utilization of nanosized particles is shown to: (1) shorten the initiation; (2) shorten burn times to increase the completeness of the combustion and therefore, to improve specific impulse; (3) enhance heat-transfer rates from higher specific surface area and; (4) enable new fuel/propellants mixture with desirable physical and energetic properties. Moreover, the nanoscale control of their synthesis together with their tuned properties authorizes new perspectives for their use, for instance, as solid fuels in automotive engines [KLE 05].

Different techniques have been developed for synthesizing nanopowders of different natures, sizes and shapes, but the emphasis is put on nanopowders of aluminum which are mostly used in practice to dope propellants, explosives and pyrotechnics. It offers a reasonably high-energetic density source and is also largely available in the Earth's crust for the benefit of mass production capability [STA 10, REE 12, WAN 13, DUB 07]. The oxidation of aluminum to alumina (Al_2O_3) releases -31.1 kJ/g [LID 91]. By comparison, CL-20 ($\text{C}_6\text{N}_{12}\text{H}_6\text{O}_{12}$) has an enthalpy of combustion of 8 kJ/g [SIM 97]. Boron is also a good choice as an additive since the oxidation of B into B_2O_3 releases -58.9 kJ/g; however, the presence of the low melting oxide on the particle surface and the formation of hydrogen boron oxygen (HBO) intermediate species (HBO, HBO_2) slow the combustion and in consequence, the rate of energy release.

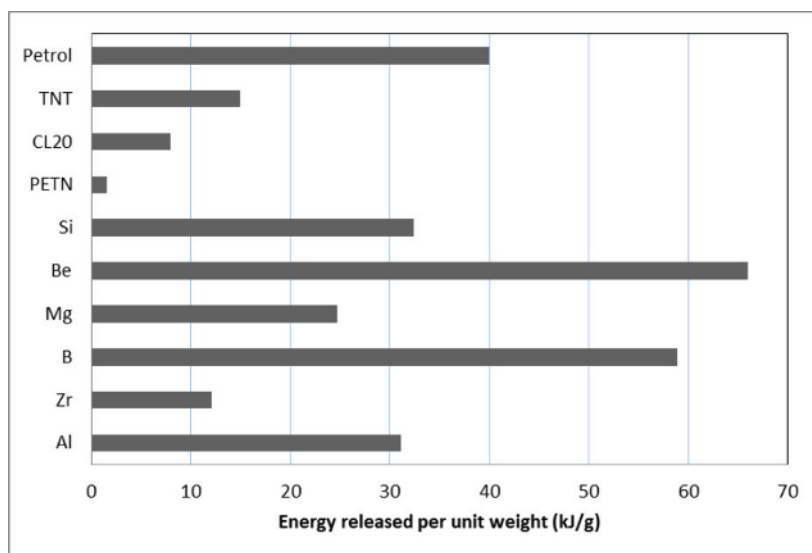


Table 1.1. Maximum enthalpies of combustion for selected monomolecular energetic material in comparison to a few metal fuels

1.1. Al nanoparticles manufacturing

The rapid acceleration of research in the area of nanoenergetic materials is mainly connected to the progress made in the manufacturing of Al nanopowders that made it possible to increase and multiply the number of research experiments in laboratories, more than a decade ago. In the following, we discuss the different methods for producing Al metallic nanoparticles that can be classified into three distinct categories: (1) those based on vapor-phase condensation; (2) those based on liquid phase chemistry and to a lesser extent; (3) those based on mechanical methods.

1.1.1. Vapor-phase condensation methods

1.1.1.1. Electrical explosion and vaporization wire

Most of the studies describing Al nanoparticles or including them into composite energetic materials use Al nanopowders synthesized by electrical explosion wire (EEW) process under diverse atmospheres. The method,

which has its roots in the work of Narme and Faraday (1774), has been pioneered for metal nanoparticles fabrication by Russian scientists starting in the late 1980s [DOL 89] and continues to be developed around the world since then [SED 08, IVA 03, JIA 98, KWO 01, SAR 07]. The electrical explosion is accompanied by shock-wave generation and rapid heating of the metal to a temperature of 10^4 °C at a rate of more than 10^7 °C/s. The underlying physics of the wire explosion remains the subject of current investigations. However, there is consensus in the fact that an explosion occurs forming a plasma. This plasma is spatially restricted by a very high field created by the pulse. When the metal vapor pressure exceeds the cohesive force of the metal, there is an interruption in current flow, causing the plasma to generate clusters of metal that are projected at supersonic speeds in the environment. EEW technology is used to produce nanopowders of Al, Ti, Zr, Mg and other metals with a particle size of 40–100 nm and a specific surface area of 10–50 m²/g. The method is employed on a large scale with a production capacity of a few hundreds of grams per hour with a rate depending on the metal type.

Even if the process is performed in an inert atmosphere (e.g. He, Ar or Xe), pure aluminum being pyrophoric, the aluminum particles are spontaneously passivated with a thin alumina layer. This natural thin alumina layer that is formed spontaneously at low temperature is amorphous with a thickness ranging from 0.5 to 4 nm. Most of the experimental data on commercial Al particles give a thickness ranging from 2 to 3 nm. A way to control the thickness of the particle oxide layer is to passivate the nanoparticles with a controlled protective oxide (see Figure 1.1) just after the nanoparticle formation to effectively hinder further oxidation during their storage. Practically, the as-grown aluminum nanoparticle will be very sensitive to whatever oxidizing atmosphere leading to different alumina layers in nature and thickness, such as the formation of hydroxide. The control of this passivation phase is commonly accomplished as a separate processing step, in which the chamber filled by inert gas for powder production is evacuated and refilled with an oxidizing gas mixture. Typically, a dry oxidizing atmosphere with low partial pressure of oxygen (e.g. 0.01% of the total pressure) is sufficient to control the passivation. Alex® is a leading manufacturer of powders produced by the EEW technique [SAR 07, TEP 00]. Characteristic transmission electron microscope (TEM) images of ALEX® aluminum nanopowders obtained by wire explosion process are shown in Figure 1.2.

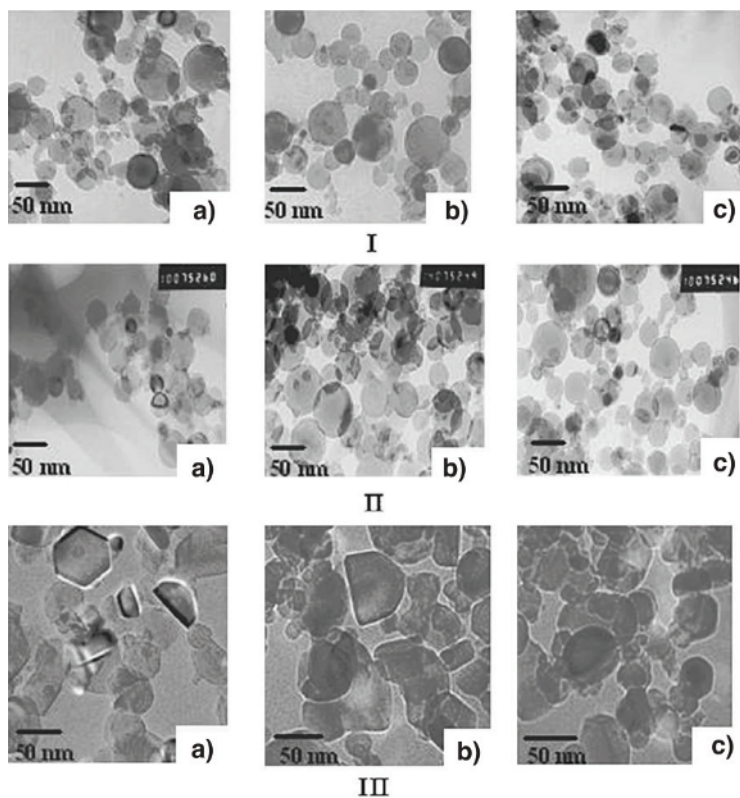


Figure 1.1. Transmission electron microscopy images of aluminum nanoparticles produced in different atmospheres: (I) helium, (II) argon and (III) nitrogen and for different oxygen pressures a) 0.025 MPa, b) 0.05 MPa and c) 0.1 MPa [SAR 07] (Copyright 2007 Elsevier)

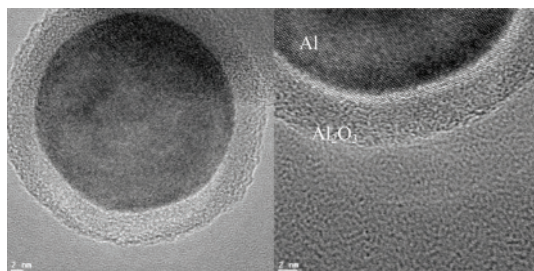


Figure 1.2. Transmission electron microscopy images of ALEX® aluminum nanoparticles. Pure aluminum core coated with a 3–4 nm alumina shell is observed

Aluminum nanopowders can also be produced from condensed aluminum vapor generated when a thin aluminum wire is vaporized by a strong electric current passing through it. After condensation, the particles are collected on the walls of the explosion vessel. Nanoparticles of many other metals and alloys can also be obtained such as Cu, Ni, Fe, Cu/Zn, TiO₂, TiN, Fe₂O₃, etc. [TEP 00, WAN 01a, KWO 05, WAN 01b, NAK 98]. The effects of pressure, gas environment, electric pulse characteristics and other experimental parameters have been widely studied [JIA 98, IVA 03, KWO 01, SAR 07]. It was demonstrated that a higher pressure results in the formation of coarser particles. It was also reported that an increased pressure of the inert gas results in an increased yield of aluminum nanoparticles. This synthesis procedure enables to produce the Al nanopowders in different environments. By varying the composition and concentration of the atmosphere, the composition of the passivation layer can be tuned. For example, aluminum particles coated with a thin layer of AlN, Al(OH)³ or *n*-Al₄C₃ can be obtained by performing vaporization or electrical explosion in a nitrogen–argon gas mixture or water or decane. Other passivation layers have also been considered as fluoropolymers, stearic and oleic acids, and aluminum diboride [GRO 06b, KWO 03a]. In Figure 1.3, we see the two-layer coating of organically passivated Al particles. A detailed section on passivation layer is proposed later on in the book.

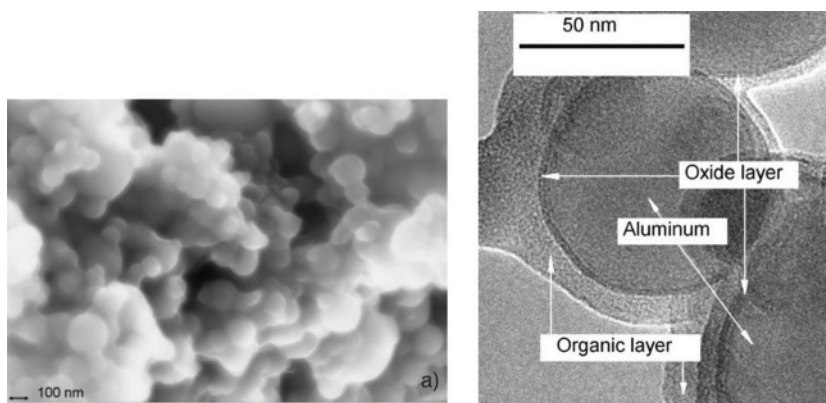


Figure 1.3. Scanning electron microscopy images of aluminum nanoparticles passivated by steric acid [GRO 06b] (Copyright 2006 Wiley)

Electro-exploded wires technology presents the advantages of being simple, efficient and well-adapted to producing large quantities of nanoparticles. The sizes of the obtained particles typically vary over a fairly broad range from 40 to 100 nm. The control of the size and shape of the particles are operated through the adjustment of the energy passing through the wire for its vaporization and the use of a suitable medium [WAN 01b, NAK 98].

1.1.1.2. *Other techniques*

A couple of other techniques for the production of Al nanoparticles have been proposed and used. The evaporation of bulk aluminum samples or aerosolized micron-sized powders followed by controlled vapor condensation has been discussed in the literature [GRA 76, SCH 06, PIV 06, CHA 06]. A crucible containing bulk aluminum is heated until vaporization in a flowing inert gas environment. The heating can be performed through several different protocols: radiative heaters, induction heaters, lasers, electric arcs or special high temperature furnaces. The pressure and nature of gas during condensation contribute to the determination the particle characteristics: a low pressure (less than 1 kPa) inert gas results in the formation of nanoparticles, while high pressures result in increased particle sizes. Additionally, condensation of metal vapors in lighter inert gases (e.g. He, Ar or Xe) is shown to produce finer particles.

Cryogenic melting of metals [BRE 08] is another effective method for producing metal nanopowders. In this case, metal particles are formed as a result of spontaneous condensation of metal vapor in a cryogenic liquid. Metal vapor is produced by rapid induction heating of a metal rod due to a powerful high generator. This heating method produces high vapor pressure in a very short period. The cryogenic liquid is continuously fed into the reactor, and nanoparticles are formed by rapid condensation of the saturated metal vapor. The low temperature of the medium provides a high rate of particle formation and rapid cooling. A diameter less than 70 nm has been demonstrated. The method is particularly used for metals with high melting points.

1.1.2. *Wet chemistry*

Wet chemistry techniques are attractive for the commercial synthesis of aluminum nanopowders because of their setting-up simplicity, the inherent safety of handling the reactive powder under liquid and the ability to functionalize the particle surface during the manufacturing process. In

[HIG 01], Al nanopowders were prepared by decomposing alane-adducts in organic solvents under an inert atmosphere. Effective adduct species were reported to include trialkylamines, tetramethylethylene-diamine, dioxane and other aromatic amines and ethers. Highly uniform particles were obtained with particle size selectable in the range of about 65–500 nm by adjusting the catalyst concentration and by varying the concentration of the adduct species. As is typical for all reported wet chemistry techniques, the methodology is based on careful and slow mixing of measured amounts of the starting solutions followed by continuous stirring and drying of the product. Such a methodology is not well suited for mass production and substantial modifications are necessary to obtain practical quantities of the desired reactive nanopowders. As a result, to date, there is no commercial mass production of aluminum nanopowders produced by wet chemistry techniques.

1.1.3. Mechanical methods

Milling processes can be an alternative to gas condensation methods or wire electro-explosion processes to prepare highly reactive particles. In [AND 13], Andre *et al.* proposed mechanical milling approach for the synthesis of reactive aluminum nanoparticles. Milling techniques are currently explored for the manufacturing of nanostructured powders with enhanced properties in comparison to micro-sized particles for different types of materials [PAT 12]. These mechanical methods are well adapted for the generation of aluminum nanoparticles due to the high ductility of aluminum material. The introduction of oxygen during milling enables us to obtain powders with high specific areas: specific surface area obtained is for the best around 20 m²/g, but the nanoparticle shape is not spherical. Interestingly, the core aluminum is poly-crystalline (see Figure 1.4) and the amorphous alumina shell thickness is superior to the one obtained with previously presented methods. Specifically, Andre *et al.* have measured a thickness of 4.5 +/-0.5 nm for Al nanopowders synthesized using a milling technique in the following conditions. Powder from AlfaAesar¹ (purity of 99.8%) was milled using a high-energy planetary ball milling equipment. The rotation speeds of vials and plateau were 800 rpm (round per minute) and 400 rpm, respectively, in opposite directions for a total milling time of 16 h. A

¹ <https://www.alfa.com/>.

controlled quantity of air (71 cm^3) was added in order to monitor the thin alumina layer formation.

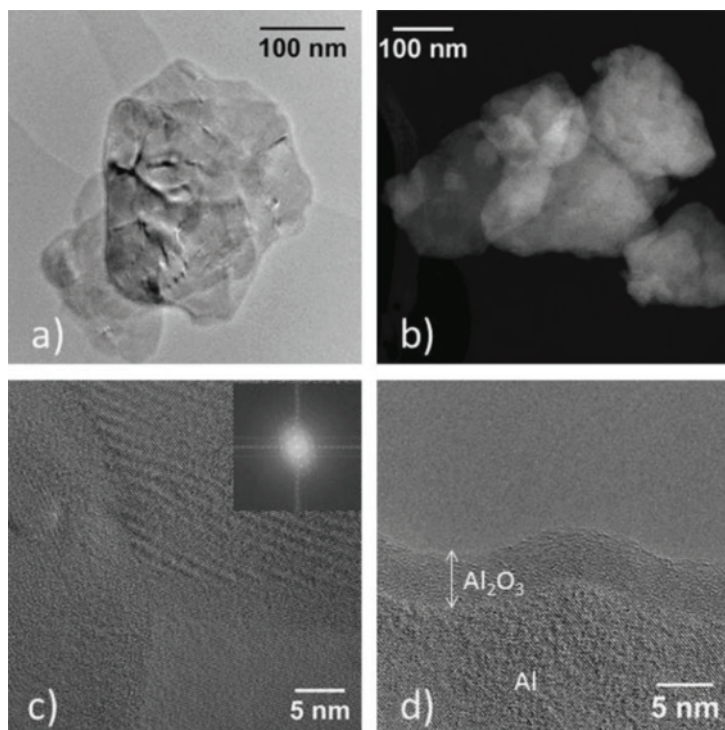


Figure 1.4. Transmission electronic microscopy images of aluminum nanoparticles obtained by high-energy ball milling: a) aggregation of particles; b) zoom on the aluminum core poly-crystallinity; c) zoom on the amorphous alumina layer [AND 13] (Copyright 2013 Elsevier)

One of the main differences with nanoparticles obtained by vapor-phase condensation is the presence of alumina at the grain boundaries.

1.2. Example of Al nanoparticles passivation technique

The surface passivation of aluminum particles is of crucial importance for safety and handling purposes as well as for its impact on thermal properties and energetic performance. As previously mentioned, pure aluminum being pyrophoric, the aluminum particles are spontaneously passivated with a thin

amorphous alumina: from 0.5 to 4 nm in thickness depending on the time of exposure with oxygen (mainly linked to the storage time). Current research on Al nanopowder is focused on preparing high-quality and well-passivated powders [FOL 05b, JOU 05b] following different strategies detailed in the next sections. The goal for all the studies is to develop passivation coatings that can protect particles from oxidation when stored in air without affecting the particle burning properties. Furthermore, preventing the formation of further alumina passivation layer increases the purity (i.e. rate of pure aluminum over the entire product) of the powder guaranteeing the reliability of its energy reservoir. Typically, Al particles made from vapor condensation, passivated with a native thin alumina, have purity ranging from 42 to 81% depending on the particle diameter ranging from 20 to 80 nm, considering a passivation shell thickness of 2 nm. With a passivation coating preventing spontaneous oxidation, the metal content in the powder can reach 95–98 wt.% of metal Al and therefore, increase considerably the percentage of pure aluminum per unit of mass. We can distinguish metal-based passivation layers and organic coatings.

1.2.1. *Metallic coating*

For example, surface layers of transition metals were formed on Al nanoparticles to prevent them from oxidation in air [FOL 05, GAO 07]. In [FOL 05], aluminum nanopowder was synthesized by thermal decomposition of an alane solution in the presence of a titanium catalyst under an inert atmosphere. In [GAO 07], the nanopowder was formed upon mixing and drying of aluminum dissolved in NaOH co-mixed with a nickel salt solution. In both cases, aluminum nanoparticles served as a reducing agent for the transition metal complexes so that reduced metal films were produced on the aluminum surface.

1.2.2. *Organic coating*

In a different passivation approach, aluminum nanopowders coated with non-metallic self-assembled monolayers (SAMs) were prepared in [JOU 05a, JOU 06]. Nanoscale Al particles were produced in solution by the catalytic decomposition of $\text{H}_3\text{Al.NMe}_3$ or $\text{H}_3\text{Al.N(Me)Pyr}$ by $\text{Ti}(\text{O}^i\text{Pr})_4$ (see [JOU 05b] for details) and coated *in situ* using a perfluoroalkyl carboxylic acid SAM. The Al particles were coated directly in solution and therefore, were not exposed to oxygen. It was observed that the SAM coating passivated the aluminum preventing the oxidation of the particles once

exposed to air. Contrary to alumina-coated nanoparticles, it makes the nanopowder soluble in polar organic solvents such as diethyl ether [JOU 05b, JOU 06]. The obtained composite particles (Al coated with organic) are shown in Figure 1.5. The protective layer is clearly fairly thick resulting in the overall reduction of the energy density of such materials.

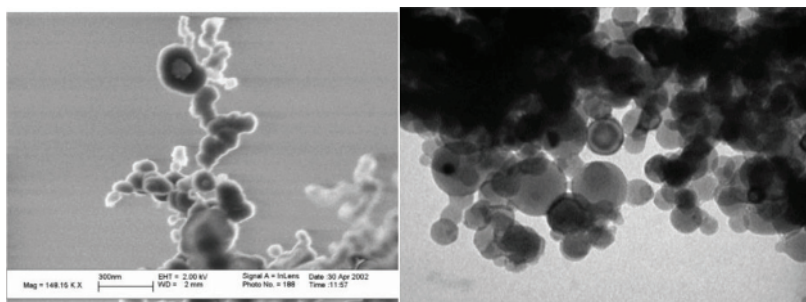


Figure 1.5. Scanning electronic microscopy images of the $Al/C_8F_{17}COOH$ composite at 148 000 magnification and $Al/C_{13}F_{27}COOH$ composite at 200 000 magnification [JOU 05b] (Copyright 2005 American Chemical Society)

New approaches to passivating the surface of Al nanoparticles continue to be developed and substantial progress is expected in this area in the near future. For example, encapsulation of aluminum nanopowders in polystyrene was recently described in [ZHA 07] and was shown to be effective in preventing aluminum oxidation.

In [PAR 06], Rai *et al.* studied the properties of carbon as a passivating layer, by using either a laser ablation method or a direct current (DC) arc to create, and coat aluminum nanoparticles in a continuous manner. The carbon coating was created by injecting ethylene (C_2H_4) into the plasma created by the laser. As a result, the aluminum nanoparticles were coated with a carbon layer of thickness around 1–3 nm. Below $700^\circ C$, the coating was stable. However, the carbon coating oxidized above $800^\circ C$.

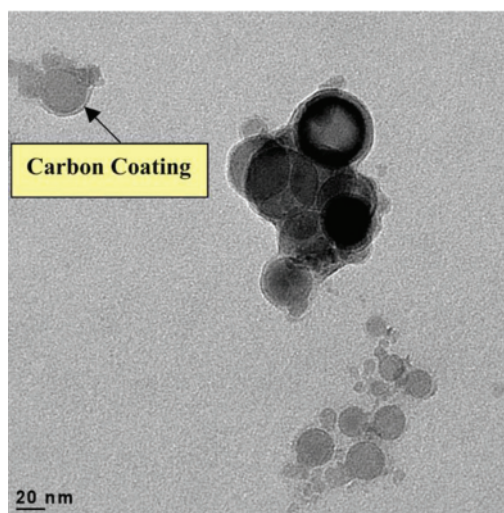


Figure 1.6. Transmission electronic microscopy images for coated aluminum nanoparticles obtained by DC arc method [PAR 06] (Copyright 2006 Springer)

1.3. Characterization of Al nanoparticles properties

The key properties of aluminum nanopowders to be known before any use in energetic mixtures or for energetic applications include particle size, size distribution, particle morphology, chemical composition, nature and thickness of the passivation layers and the percentage of pure metal. These data are of primary importance in determining the reactivity and ignition temperature of the Al powder. Various methods exist to unravel nanoparticle structures and measure powder size distribution. This section presents the different techniques and methods found in the literature to picture aluminum nanopowder structures and to subsequently study their thermal response in the context of energetic materials.

The size and particle morphology, the size distribution can be obtained by electron microscopy as, for example, scanning electron microscopy (SEM) and TEM. They are common tools and practices to determine the particle shape, size and give information about the particle surface morphology (see Figures 1.6 and 1.7). In order to be representative, such measurements must consider a large number of particles and different locations of the sample. The determination of particle size distribution is then carried out by image

analysis. In general, a powder is considered monodisperse when the diameters of the individual particles fall within 10% from each other.

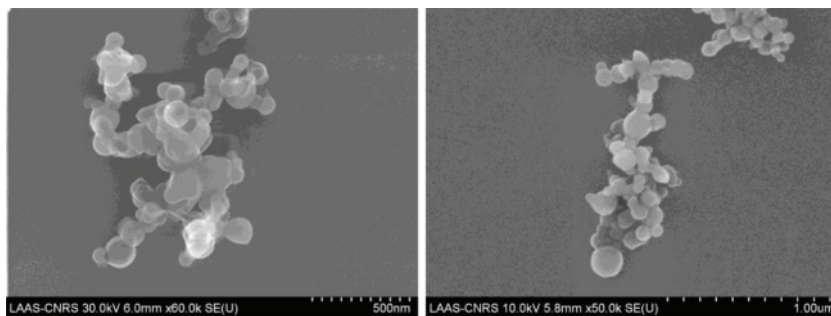


Figure 1.7. *Scanning electronic microscopy images of nanometer aluminum particles*

High resolution transmission electron microscopy (HR-TEM) is also successfully used to characterize the oxide coatings present on aluminum particles exposed to different environments. As an illustration, we can go back to Figure 1.2 showing the Al nanoparticle core and its surface passivation layer, many other examples can be found in published papers [GRO 06a, RUF 07, RAM 05, SEV 12]. Crystallinity, microstructure and homogeneity of the oxide layers are inherently difficult to measure due to their overall amorphous nature.

1.3.1. *Light scattering methods*

Particle sizes can also be quantified using laser light scattering (LS) and several commercial instruments utilizing this technique are available. Low-angle light scattering (LALS) is the only LS technique that actually measures a scattered light intensity that is due to the interaction between a single particle and an incident light. The scattered light intensity is thus directly proportional to particle diameter and weight. The scattering behavior is also dependent on the light wavelength. These instruments are generally designed for size characterization of micron-sized powders or their aggregates. However, they are also capable of measuring smaller sizes, typically down to the 50–100 nm range due to specific algorithms for processing the scattered laser emission spectra. The main advantage of this type of measurement is that a powder with relatively broad particle size distribution can be characterized. However, for accurate measurements, the optical properties of

the material surfaces need to be known. Such properties are not well established for many materials, especially for the nanosized particles for which, as noted above, the material properties are expected to substantially differ from those of the respective bulk materials.

Another group of laser LS devices is the dynamic LS or photon correlation spectroscopy. A laser light is focused into a suspension. It determines the particle size by measuring the rate of fluctuations in laser light intensity scattered by particles which have been dispersed in a liquid [BAR 84, PEC 85]. The Brownian motion of particles in suspension causes laser light to be scattered at different intensities. Analysis of these intensity fluctuations gives the velocity of the Brownian motion and hence, the particle size using the Stokes–Einstein relationship. The measurement needs to be processed assuming the viscosity of the fluid, a specific shape of the size distribution function, so that generally the mean particle size and the width of the particle size distribution can be quantified. Dynamic LS technology offers many advantages such as accurate repeatable particle size analysis in short time and reduced sample size.

1.3.2. Gas adsorption method: specific surface measurement, BET diameter

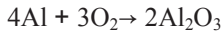
Besides electron microscopy, one common characterization technique for the determination of particle size is based on the volumetric adsorption of a gas on a sample of particles that provide a measurement of the specific surface of these particles. Surface areas are calculated using so-called Brauner, Emmett and Teller (BET) theory. Usually, the surface area measurements are determined by nitrogen adsorption using a gas adsorption analyzer. The “BET diameter” assumes that the measured specific surface of a powder is equivalent to that produced by monodisperse spherical particles, which is not necessarily the case in nanopowders [MOO 07, PRE 05]. This technique and associated theory are well known, widely used and a few commercial devices are available. The BET method is shown to provide more accurate experimental data on ultra-fine particle samples.

1.3.3. Thermal analysis: purity or aluminum content percentage and oxide thickness

Thermal analysis techniques are widely used for the characterization of energetic materials, especially differential scanning calorimetry (DSC) and thermogravimetry analysis (TGA). In this latter technique, a small amount of

powder, typically 5–10 mg, is placed in a crucible and is heated at low heating rate (5–40°C/min) under flowing air or mixture of Ar and oxygen gas. The sample is weighted before and after the analysis. For DSC, after the first heating cycle, the sample is cooled down to room temperature and then heated again at the same heating rate. This second analysis is used to correct the baseline. It is assumed that the bulk heat capacity of the sample does not change between the first and the second heating run. Note that thermal analysis relies on assumptions about the density, structure and homogeneity of the natural passivation layer. The sample has to be well characterized before thermal analyzing with respect to its detailed chemical composition, its particles size, its size distribution, etc., to ensure a good thermal measurement accuracy. In practice, a sufficient number of repeated measurements are required.

Figure 1.8 shows a typical TGA curve of the Al nanopowder oxidation in Ar + O₂ environment in the temperature range of 30–1,000°C at a heating rate of 10°C/min. The active aluminum content can be easily obtained from mass gain measurement in a thermogravimetric analyzer. The mass gain $\Delta m(\%)$ in the TGA under Ar/O₂ mixture (typically, 75/25 mixture) is attributed to oxidation of active aluminum:



The aluminum content, or purity P , can be calculated using the following equation based on the mass balance and the mass ratio of aluminum to oxygen in Al₂O₃:

$$P = \frac{108}{96} \Delta m(\%) \quad [1.1]$$

P is typically between 41 and 80% for particle size ranging from 20 to 80 nm and considering an oxide shell thickness of 2 nm. Knowing P and the total particle diameter d , the thickness of the oxide layer (t_{oxide}) is calculated by equation [1.2]:

$$t_{oxide} = \frac{d}{2} \sqrt[3]{1 - \frac{P \times \rho_{\text{Al}_2\text{O}_3}}{m_{\text{Al}_2\text{O}_3} + P \times (\rho_{\text{Al}_2\text{O}_3} - \rho_{\text{Al}})}} \quad [1.2]$$

with $\rho_{\text{Al}_2\text{O}_3}$ (3.05 g.cm⁻³) and ρ_{Al} (2.7 g.cm⁻³) being the densities of amorphous aluminum oxide and aluminum at room temperature, respectively. Note that it is assumed that Al₂O₃ is amorphous with a density of 3.05 g.cm⁻³.

However, it has been reported that the alumina passivation layer can be porous, partially hydrated and certainly non-uniform in thickness [SEV 12, BAR 84]. Recent research using prompt gamma neutron activation analysis and HR-TEM [GAO 07] showed that the amorphous oxide coatings on aluminum nanopowders can also include impurities of hydroxide, trapped water molecules and boron. The oxide thickness can be determined by HR-TEM images combined with particle size distribution measurement.

The combination of multiple characterization tools (DSC, TGA, TEM...) makes it easier to properly estimate the gravimetric fraction of pure Al in the powder, P . Data from TGA curves can be also used to determine activation energies [AUM 95], pure or active aluminum content [JOH 07], oxide layer thickness [EIS 04] and particle size.

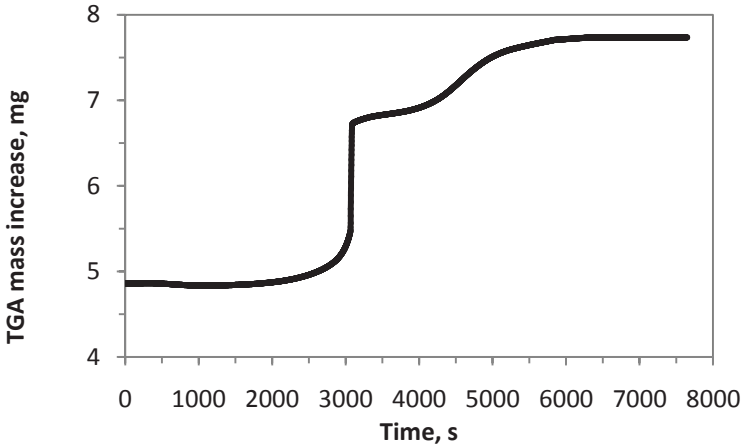


Figure 1.8. TGA curves of aluminum nanopowder in Ar/O₂. The TGA scans were performed at 10°C/min under 25/75 O₂/Ar atmosphere

1.3.4. Chemical analysis

Chemical analysis using induced coupled plasma (ICP) emission is another tool that enables us to determine the purity of nanopowder as well as the Al/Al₂O₃ ratio. The metallic Al content is derived from the oxygen content by assuming that oxygen is only present in the oxide passivation layer.

1.4. Oxidation of aluminum: basic chemistry and models

In this section, we consider aluminum powder oxidation under low heating rate, e.g. $< 40^{\circ}\text{C}/\text{min}$. It is now well established that oxidation of nanopowders begins at much lower temperatures than their micron size counterparts. The oxidation rate of Al depends on the temperature of the material and can be represented on the typical curve given in Figure 1.9.

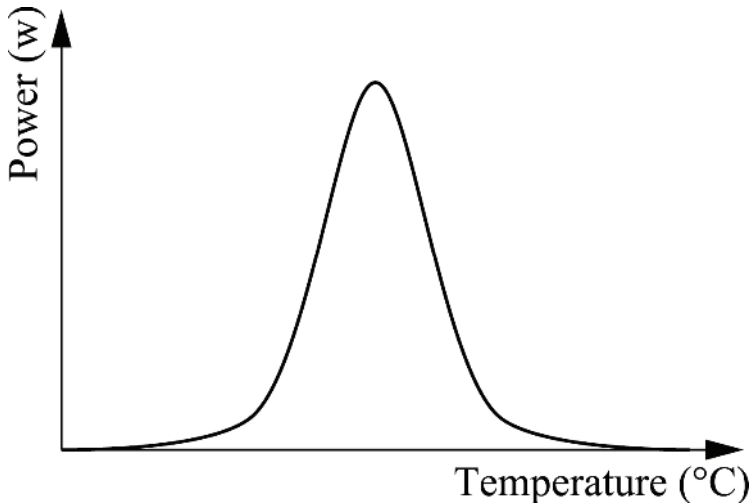


Figure 1.9. *Typical DSC curve of the aluminum oxidation in O_2/Ar oxidizing environment*

The complex oxidation process leading to the formation of the alumina passivation layer is still not well understood but few chemical reactions and phenomenological mechanisms responsible for oxidation have been proposed in the literature to fit the experimental results. They will be presented in the following sections.

1.4.1. Initial stage of aluminum oxidation from first principles calculations

The early stage of aluminum oxidation ($n = 0$) has attracted much interest because of its practical importance and also because it was considered as a model system to understand the fundamentals of the oxidation of metallic surfaces. On the experimental side, the first comprehensive picture of the

aluminum oxidation at early stages and its different regimes was given by Brune *et al.* in the early 1990s with the help of STM experiments [BRU 92, BRU 93]. At low coverage (a few Langmuir) and room temperature, molecular oxygen exhibits dissociative chemisorption. The oxygen atom separation following the dissociation is shown to be enhanced by their hyperthermal motions because of the exothermic nature of the chemical decomposition reaction. This process is accompanied with surface diffusion leading to the formation of oxygen (1×1) patterns, i.e. clusters of adsorbed oxygen atoms on high surface symmetry hollow sites. Increasing the coverage, but still long before the oxygen (1×1) monolayer coverage, oxidation starts to occur at the oxygen cluster sites. This means that a mixing of both aluminum and oxygen species is initiated. Since the thermodynamics of the adsorption and formation of oxygen (1×1) clusters plus proposals of potential interfacial oxide/Al structures have been proposed theoretically by density functional theory calculations [BEN 03, JAC 95, RUB 02, KIE 01, KIE 02, CIA 04], a mechanistic description of these observations has come to an end only very recently [LAN 12, LAN 14]. Indeed, it was trivially expected that oxidation process was driven by oxygen penetration into the aluminum substrate or subsurface [ZHU 03] leaving unclear the kinetics and associated pathway for this penetration as well as conditions for this penetration to occur, i.e. at which oxygen coverage and through which atomistic environment. Also, controversial discussions were oriented on the initial coverage value necessary to observe oxidation nucleation [CIA 04]. Lanthony *et al.* confirmed the Brune's STM observations that the oxygen (1×1) clusters were promoting oxidation. They also demonstrated that oxidation nucleation was due to additional incoming of oxidizing species on the outer surface of the oxygen (1×1) clusters making some aluminum atoms underneath the oxygen cluster to "percolate" through it up to the surface. This complex chemical process has been called "extraction" mechanism and its different stages are illustrated in Figure 1.10 when the surface is exposed to atomic oxygen. Importantly, this process is barrierless indicating that oxidation will take place spontaneously as soon as oxygen clusters are formed and exposed to further gas phase oxidizing species. It is shown that under higher coverage, multiple barrierless extractions can be operated, up to the stripping or oxidation of about two layers of the aluminum surface. This leads to the formation of a native and stable aluminum oxide layer. Continuing the oxidation process necessitates activation and other chemical mechanisms that are still to be determined in order to completely understand passivation layer formation.

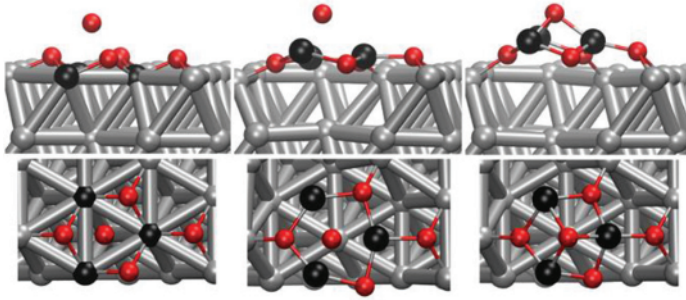


Figure 1.10. DFT structures of Al “extraction” mechanism: side views on three top images, top views at the bottom. Extracted Al atoms are the biggest in black, O atoms are the smallest in dark gray, gray spheres are aluminum atoms

1.4.2. Thermodynamic modeling of Al oxidation under low heating rate

At the experimental level, the oxidation thermodynamics are explored by combining several techniques. As already mentioned, the oxidation steps are characterized using TGA analysis in oxygen/argon (25/75) environment from room temperature to 1,300°C. The TGA curve gives the mass gain resulting from the oxidation process, and simultaneous DSC measurements can be added to quantify the corresponding exothermic effects as well as to detect phase transitions. The structure and nature of the powders can also be checked before and after thermal treatments by X-ray diffraction or Raman analysis. These experimental results [JOH 07, MEN 98b, JON 00] are generally consistent between each other and show that for particles of 100 nm and finer, the oxide is mostly formed below the bulk aluminum melting point, between 450 and 605°C and with a higher degree of reaction.

The controversy arises during the interpretation of the results since the real mechanism responsible for the oxidation rate of aluminum nanopowders is still not well understood. Some suggest that the Al core expands and breaks the shell ejecting small molten clusters of Al at high velocity [UME 07]. Others suggest that aluminum from the core and oxygen from the outer surface atoms diffuse and meet to react within the passivation layer. This is discussed in the following and will be reviewed in more detail in Chapter 5.

1.4.2.1. Fixed ignition temperature model

The simplest and first ignition model found in the literature is based on a number of experimental reports showing that large aluminum particles

(> 10 μm in diameter) ignite close to the melting point of Al_2O_3 (i.e. 2,042°C) [BOI 02, BRO 95]. Hence, it was suggested that the oxide film that is always present on the aluminum surface prevents ignition until it starts melting. This melting results in the formation of isolated oxide islands in replacement of the previous continuous coating film. The surface of aluminum is then exposed to the oxidizer and the particle ignites. Therefore, the description of aluminum ignition can be envisaged at a constant temperature. It has been recognized that a better agreement with experiments can be achieved in most cases if the ignition temperature is selected somewhat below the Al_2O_3 melting point in the sense that a thin and constrained protective oxide has its melting point lower than the bulk value. For experiments in which large aluminum particles (over micron size) are used, this model produced quite satisfactory results. However, this approach is inadequate for finer aluminum particles.

1.4.2.2. Stress in the oxide layer model

This model introduced by Rozenband *et al.* [ROZ 92] suggests that the protective oxide coating breaks up due to the increasing mechanical stresses during heating and core Al melting. Then the aluminum surface becomes exposed to the oxidizer and the particle ignites. This hypothesis was largely discussed: the mechanical properties of the heated alumina are poorly known. The most significant stress in the oxide film is obtained just after the melting of the Al shell composed of pure aluminum, i.e. immediately above 660°C. At elevated temperatures, e.g. above 1,100°C, the deformations of Al_2O_3 result in grain boundary sliding causing a brittle to ductile transition. Therefore, the stresses in the oxide film can be relaxed avoiding the rupture of the oxide film. This model is contested to adequately describe ignition of aluminum powders observed at low temperatures (around 500–600°C).

1.4.2.3. Oxidation growth modeling

The most conventional approach to modeling the oxidation growth kinetics is to consider a linear-parabolic regime. This approach considers that the initial growth regime is dominated by chemical reactions with the oxidizing species of the gaseous environment. The overall oxidation can be written as [FED 03].

$$\frac{dt_{oxide}}{dt} = K(t_{oxide})^{-n} C_{ox}^m \exp\left(-\frac{E}{RT}\right) \quad [1.3]$$

where t_{oxide} is the thickness of the oxide film, t is time, C_{ox}^m is the oxidizer concentration proportional to the oxidizing pressure near the particle surface

and m is the order of the reaction in terms of the oxidizer. R is the universal gas constant, and E and K are the activation energy and pre-exponent, respectively. The exponent n determines the dependence of the oxidation rate on the oxide film thickness. $n = 0$ for linear oxidation law (suitable for the first oxidation step) and $n = 1$ for parabolic law of oxidation when diffusion of oxidizing species through the oxide already formed is the limiting step for the oxidation kinetics.

In another formulation, the general kinetic equation of oxidation can be represented in dimensionless form as:

$$v_{oxidation} = k_o \eta^{-n} \exp\left(-\frac{E}{RT}\right) \exp(-k_1 \eta) \quad [1.4]$$

where $v_{oxidation}$ is the rate of the reaction, η is the degree of oxidation determined from TGA mass changes, k_o is the pre-exponential factor, E is an activation energy accounting for the oxidation chemical reaction, R is the universal gas constant, T is the reaction temperature, and n and k_1 are, respectively, exponent and coefficient constants. E and k are determined from independent sources. Typically, these values are extracted from experimental aluminum oxidation studies. Activation energy usually does not depend on particle size and is ~ 155 kJ/mol in average for aluminum oxidation. The activation energies for heterogeneous aluminum oxidation found in the literature range from 70 to 420 kJ/mol depending on the temperature range. For example, in [TRU 06], Trunov *et al.* reported activation energy of 460 kJ/mol for 950–1,300°C range and 71 kJ/mol determined for 1,600–2,000°C temperature range. k_o is found to be 2 to 5 times higher for nanopowder than for larger size powders. Note that a small change in the activation energy greatly affects the oxidation kinetics described by an exponential function. Therefore, an adequate selection of the values of E and k is critical for an accurate description of the oxidation processes of aluminum.

Experimental works showed that at the early stage of oxidation ($\eta = 0$), the reaction rate does not depend on the degree of oxidation and the process is similar to monomolecular reactions. The Oxidation process follows a linear law up to a degree of oxidation of 0.1–0.3 and leads to the rapid oxidation of the aluminum surface into a thin amorphous oxide layer. In a second stage, the oxidation process slows down and the oxidation follows a logarithmic law due to the formation of an oxide layer through which the oxidizing species must migrate toward the interface with pure aluminum to continue the oxidation process.

Other choices have also been discussed in the literature based on the experimental data collected for different oxidation temperature ranges [KUB 62]. From this approach, the heat release due to the oxidation is estimated and compared to external particle heating or heat losses. Ignition can, therefore, be predicted by an adequate particle heat transfer model including the enthalpy of oxidation. However, the analysis of the literature shows great discrepancies between the values reported and used by different researchers.

1.4.2.4. Diffusion based on phase transformation processes

Recent research on aluminum particle ignition has proposed that the oxidation is controlled by non-constant diffusion processes of oxygen and aluminum through the surface oxide coating. Importantly, it is assumed that the diffusion is critically affected by polymorphic phase changes occurring during heating. Trunov *et al.* [TRU 06] suggested that the oxidation under low heating rates ($< 40^\circ\text{C}/\text{min}$) is caused by a sequence of polymorphic phase transition occurring in the oxide layer: amorphous $\text{Al}_2\text{O}_3 \rightarrow \gamma \rightarrow \delta \rightarrow \theta \rightarrow \alpha \text{Al}_2\text{O}_3$

The densities of these alumina polymorphs are different from each other, as shown in Table 1.2.

	Density, g/cm^3
Amorphous Al_2O_3	3–3.1
$\gamma\text{-Al}_2\text{O}_3$	3.6–3.67
$\alpha\text{-Al}_2\text{O}_3$	3.99

Table 1.2. Density of different alumina polymorphs

The overall phase transformation process can be explained as follows. After the first oxidation step (formation of a thin amorphous oxide), the thickness of the natural amorphous alumina layer increases slowly. Around 550°C , this layer exceeds the critical value of about 4 nm and becomes metastable. A transformation into $\gamma\text{-Al}_2\text{O}_3$ then takes place. This phase transformation can reduce the thickness and the diffusion resistance of the oxide layer. For thin oxide layers observed at high heating rates, this phase change can also result in local discontinuities in the oxide coverage. The resulting $\gamma\text{-Al}_2\text{O}_3$ is stabilized due to its small crystallite size. This amorphous to $\gamma\text{-Al}_2\text{O}_3$ phase transformation can lead to a small mass increase because the density of the oxide layer increases. The growth of a continuous $\gamma\text{-Al}_2\text{O}_3$ layer and its partial transformation into $\theta\text{-Al}_2\text{O}_3$

polymorph takes place in a third stage after the melting point of Al (660°C). Finally, the fourth stage corresponds to the high temperature oxidation above 1,100°C and leads to the formation of α -Al₂O₃. The transformation to thermodynamic stable α -alumina may proceed directly or via a number of intermediate phases such as δ - and θ -alumina.

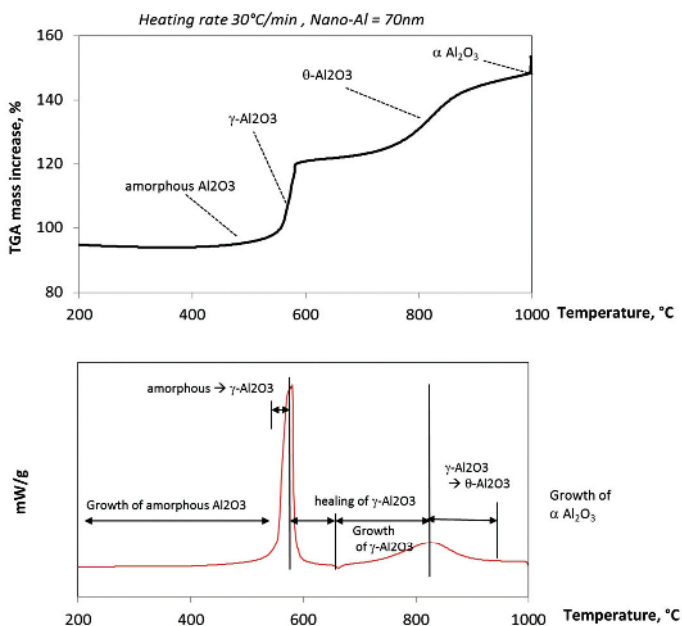


Figure 1.11. An example of TGA curve showing the different aluminum oxidation stages (according to [TRU 06] description)

The sequence of alumina phase transformations described above has made it possible to interpret the observed stepwise powder oxidation as pictured by experimental characterization such as a TGA experiment (see Figure 1.12). Five steps need to be analyzed to describe the oxidation quantitatively: (1) growth of the amorphous oxide, (2) the amorphous to γ -Al₂O₃ phase change, (3) growth of γ -Al₂O₃, (4) γ -Al₂O₃ to α -Al₂O₃ phase change and (5) growth of α -Al₂O₃. As an illustration, a TGA curve of the mass increase in an aluminum nanopowder heated in the thermal analyzer in argon and oxygen environment is given in Figure 1.12 indexed with the different direct oxidative growth and phase transformations. At each step, the oxide polymorphs are mentioned.

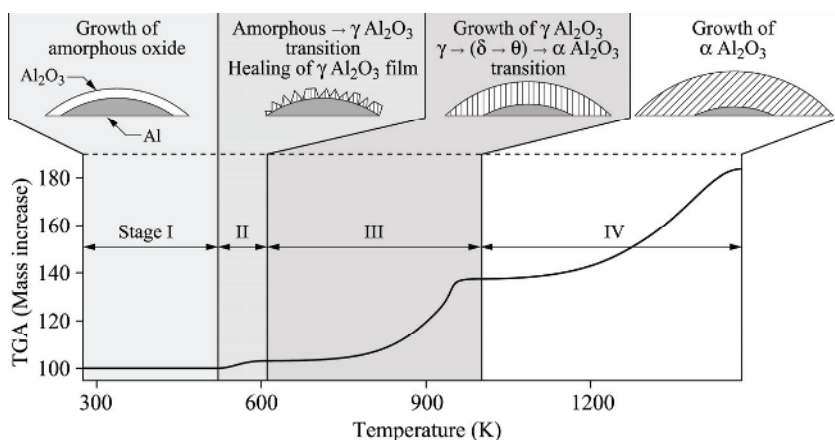


Figure 1.12. Different stages of oxidation and the respective changes in the growing alumina scale are shown schematically [TRU 06]

This model developed by Trunov *et al.* can predict that particles of different sizes ignite at different temperatures. The model consistently interprets a wide range of the previously published experimental data describing aluminum ignition.

1.5. Why incorporate Al nanoparticles into propellant and rocket technology?

It is now widely demonstrated that replacing the metal powders traditionally used in energetic mixture and rocket technology by Al nanopowders leads to a factor of 5–30 increase in the burning rate of propellants at a constant mass content of the components. This is primarily due to the following factors:

- increased reactivity of nanometer-size particles compared to micrometer-size particles;
- increased rate of energy release due to the lower melting point and much shorter combustion time of nanoparticles;
- favored mixing of components (aluminum and oxidizer), providing closer contact between them, which facilitates the diffusion of reactants to the surface and increases their reactivity.

1.5.1. Reduction of the melting point

Downscaling the average radius of the aluminum nanoparticles to the 5–50 nm range makes their melting response shift toward lower temperatures with noticeable decrease in the enthalpy of fusion [SUN 07]. One important factor in the reduction of Al melting temperature is the increased surface energy associated with nanoparticles. Some studies have demonstrated it theoretically and experimentally [ECK 93, WRO 67]. According to Eckert *et al.*, the melting point as a function of the aluminum particle diameter is given by the following empirical law for particle sizes strictly ranging from 12 to 43 nm.

$$T_m(\text{in K}) = 977.4 - \frac{1920}{d(\text{in nm})} \quad [1.5]$$

For larger particles, $T_m = T_b$ with T_b bulk aluminum melting temperature = 660°C.

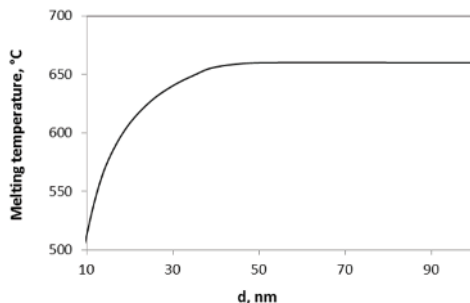


Figure 1.13. Predicted melting temperature of aluminum nanopowders as a function of particles diameter (d)

Decades ago [JON 00], Reiss and Wilson proposed a model describing the behavior of the melting point, T_m , as a function of the particle diameter d , and the oxide film thickness t_{oxide} , as:

$$T_m = T_b \left(1 - \frac{4 \times \sigma_{SL} \times 1920}{H_b \rho_{Al} (d - 2t_{oxide})} \right) \quad [1.6]$$

where T_b is the bulk aluminum melting temperature, H_b is the bulk aluminum enthalpy of fusion and σ_{SL} is the interfacial surface tension between the solid and liquid.

This model is often used and referenced in several recent papers dealing with aluminum nanopowder used in combustion systems [HUN 04, GRA 04]. The influence of the alumina passivation layer thickness has been studied by Sun and Simon [SUN 07]. The results indicated that the nature of the surface layer has no significant effect on the melting temperature.

1.5.2. Increase in the reactivity

It is observed that the reactivity of aluminum nanoparticles is considerably enhanced compared to micrometer-sized samples. Figure 1.14 illustrates the effect of aluminum size on the Al+O₂ reaction [SUN 06] where thermal analysis scans are given for 105 nm average diameter sample, 86 nm and 6 μm at a heating rate of 3°C/min under 25/75 O₂/Ar atmosphere. We clearly see that there is a large exotherm reaction peak present for the nanoparticles before reaching the Al melting peak at 660 °C. It is due to oxidation of the aluminum by O₂, whereas for the micrometer-sized particles, only a small exotherm is present prior to melting. The onset temperature for oxidation is reduced for the nanopowders. In addition, compared to a micrometer-sized sample, the melting peaks for the nanosized samples are considerably smaller, suggesting that more aluminum in the nanopowders reacted in the oxidation process prior to melting. Similar results were reported by Mench *et al.* in [MEN 98b].

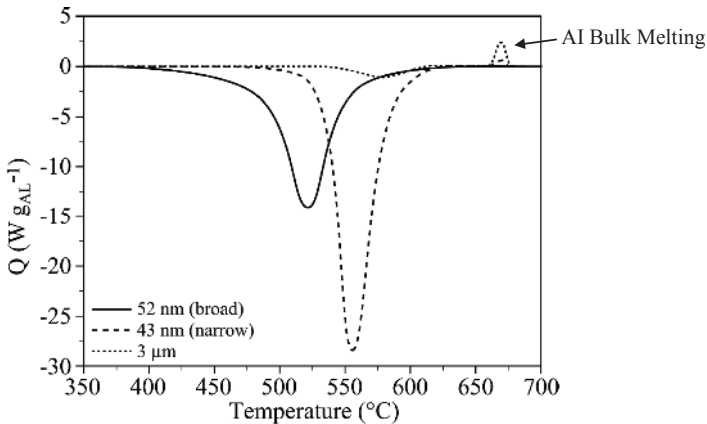


Figure 1.14. DSC curves of aluminum powder as a function of the temperature in Al/O₂ environment showing the effect of the size and size distribution of the aluminum nanoparticles. The DSC scans were performed at 3°C/min under 25/75 O₂/Ar atmosphere [SUN 06] (Copyright 2006 Elsevier)

The increased reactivity of nanoparticles is considered to be mainly related to their large specific surface area. Basically, when the particle size is reduced, the fraction of the atoms located at the surface increases. To illustrate this point, Figure 1.15 shows the surface to bulk atom ratio for a spherical aluminum crystal as a function of particle diameter. Surface atoms have free (unsaturated) bonds and a lower coordination, the bonds between surface and subsurface atoms are weaker than those between the atoms in the bulk. Atoms influence each other within approximately five interatomic distances. The thickness of this surface layer is about five atomic layers and is roughly equal to ≈ 1 nm.

Another effect typical of metal nanoparticles obtained by vapor-phase condensation technology is due to the presence of additional or excess of energy. This is due to the extremely fast formation of particles during condensation of metal vapor and the related formation of metastable and tense structures in the crystal lattice.

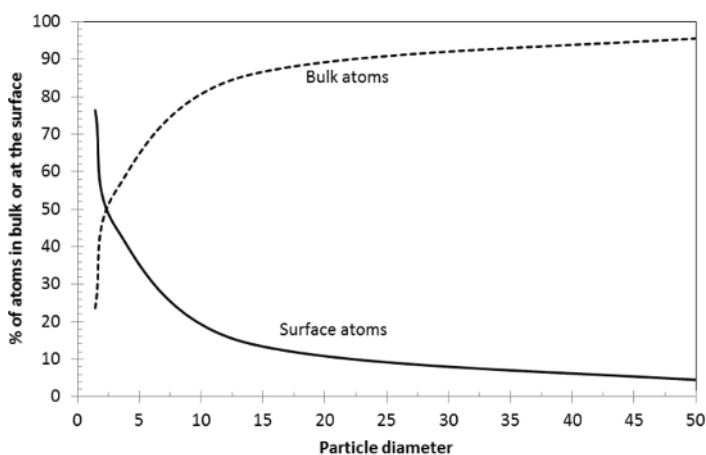


Figure 1.15. Calculated percentage of atoms in aluminum particles of different diameters (diameter of an aluminum atom is equal to 0.286 nm)